Classical rescattering effects in two-color above-threshold ionization

G. G. Paulus,[1] W. Becker,[2] and H. Walther[3]
[1]*Max-Planck-Institut für Quantenoptik, Hans-Kopfermann-Strasse 1, D-85748 Garching, Germany*
[2]*Physik-Department T30, Technische Universität München, D-85747 Garching, Germany*
and Center for Advanced Studies, Department of Physics and Astronomy, University of New Mexico, Albuquerque, New Mexico 87131
[3]*Max-Planck-Institut für Quantenoptik, Hans-Kopfermann-Strasse 1, D-85748 Garching, Germany*
and Sektion Physik der Ludwig-Maximilians-Universität München, Am Coulombwall 1, D-85747 Garching, Germany
(Received 17 April 1995)

Rescattering effects in above-threshold ionization such that the electron is driven back to the ionic core by the laser field and rescatters are considered in a completely classical framework, for a laser field consisting of a linearly polarized monochromatic fundamental and its second harmonic, as a function of their relative phase. Several features appear, owing to the two-color field: the energies of the rescattered electrons extend up to 21 U_p, with U_p the ponderomotive potential of the entire field; the angular distributions of the rescattered electrons are no longer symmetric with respect to an interchange of the backward and forward direction and more than one ring or side lobe may appear in either direction; the importance of rescattering can be deduced from the violation of a certain symmetry of the total above-threshold ionization rates for fixed energy with respect to the phase between the two fields; the spectra of the rescattered electrons change dramatically when the field intensity is raised from the multiphoton into the tunneling regime.

PACS number(s): 32.80.Rm, 42.65.Ky

I. INTRODUCTION

Ionization of atoms is an essentially quantum-mechanical phenomenon. This is affirmed by the very nomenclature used—multiphoton ionization, for moderate intensities, referring to the fact that the electron absorbs a specific (minimum) number of photons in order to become free or, on the other hand, tunneling ionization, for high intensities, asserting that tunneling at constant energy through the instantaneous barrier formed by the combined potentials is the process by which the electron gets out. Both are genuinely quantum-mechanical scenarios without any classical analog. Indeed, for not too low laser frequencies, there does not seem to exist any working classical model that would yield an understanding of the *total* ionization rates. Nevertheless, classical kinematics is capable of explaining a number of the features observed in the *shape* of the electron energy spectra of above-threshold ionization (ATI) [1]. Particularly, this is true for the high-energy region of ATI where several novel phenomena have been found recently including anomalous angular distributions [2,3] and a plateau [4] reminiscent of the plateau in high-harmonic generation. It is the interaction of the freed electron with the laser field, after the initial process of ionization, which is partly amenable to a classical analysis, and this interaction largely dominates the observed electron spectra.

Quantum mechanics does not allow, in principle, for a separation of the entire process of ionization into distinct separate steps such as the "actual" ionization coming first, followed by a redistribution of energies during the subsequent propagation through the laser field. Yet two-step models which do exactly that have met with remarkable success, both quantum-mechanical [5,6] and classical [7,8] versions, in comparison to both experimental data and numerical solutions of the Schrödinger equation. Additional support will be presented in this paper. A derivation of these models from first principles has not been given. The underlying physical picture is that, somehow, by the time the electron has reached the continuum it has largely "forgotten" how exactly it got there, and a new section in its history is beginning to unfold. The freed electron may just proceed to leave the field region, and this process is responsible for what may be called "ordinary" ATI. There is now general agreement that the newly discovered features in high-energy ATI are due to a third step: the electron returning to the ion and rescattering [2,3,9,10]. The electron may, on this occasion, equally well recombine and this is the mechanism of high-harmonic generation. The complete quantum mechanics of the electron in the field can be formulated [11] in terms of the quantum-mechanical path integral, and the latter can be constructed from the classical orbits of the electron in the field. Hence, a great deal can be learned already from the investigation of the classical orbits.

In a previous paper [12], we have used such an analysis in order to understand the anomalous angular distributions in high-energy ATI. Very similar models have been employed also in the study of classical stabilization [13]. Our results [12] showed that the pronounced side lobes that are observed in these angular distributions in a certain energy region can be attributed just to classical kinematics of electrons in laser fields. In this paper we will extend this analysis to arbitrary linearly polarized laser fields, in particular to a two-color field where one field is the second harmonic of the other. This configuration is of particular interest for several reasons. Since the two frequencies are commensurate the relative phase has physical significance. As a function of the phase, the shapes of the field and its vector potential vary considerably. As we will see below, the rate of injection of electrons in the continuum is determined by the electric field while its subsequent propagation is governed by the vector potential. For a one-color sinusoidal field, the field and the vector potential have the same functional shape and are just

out of phase by 90°. For a two-color field, on the other hand, the shapes can be very different and the relation between the maxima of the field and those of the vector potential can be controlled at will by variation of the relative phase. This allows for a much more stringent test of the two- and three-step models than is possible with just one field. Most interestingly, we will see that the high-energy ATI spectra provide what may be the most clean-cut signature for the mechanism of ionization: multiphoton versus tunneling.

There is a very substantial body of mostly theoretical work on two-color multiphoton ionization. We will here refrain from any attempt at doing justice to all these studies, using as an excuse the fact that the aspect we are interested in, viz. the rescattering effects in two-color ATI which are responsible for the high-energy portion of the spectrum, has not yet been investigated at all. However, the recent paper by Schuhmacher *et al.* [14] which extends previous work by Muller *et al.* [15] points in this direction. These authors have measured ATI spectra due to a linearly polarized laser field and its second harmonic and compared their data to calculations based on the two-step model, also known as the "simpleman's" theory [7,8]. The latter predicts that the spectra produced by two field configurations that differ by the sign of the relative phase between the fundamental and the second harmonic are identical if the forward and backward directions are interchanged. As a consequence, the total rates for fixed electron energy would be independent of the sign of this phase. The experiment, however, showed definite deviations from this symmetry, and Schuhmacher *et al.* [14] tentatively ascribed this to rescattering effects.

Rescattering effects are, of course, in principle contained in a numerical solution [16,17] of the Schrödinger equation in the two-color field environment or in a Floquet approach [18]. Since the effects are most pronounced in the high-energy part of the spectrum which is not very intense they are, however, difficult to extract from such a solution. Keldysh-Faisal-Reiss (KFR) methods [19] have been used to deal with the two-color case [20,21], but they neglect the interaction of the freed electron with the binding potential and, therefore, the rescattering effects. Model calculations such as Refs. [22] and [23] are built around the trajectories of electrons returning to the core. If extended to the two-color case they would yield a fully quantum-mechanical description of rescattering effects. The good agreement with the data which these models have achieved for one color suggests that they should work well also in more general situations.

All of the electron angular distributions to be calculated in this paper at fixed energy for the case where the frequency ratio is 2:1 will exhibit polar asymmetry. That is, unlike the case of one monochromatic field, the angular distributions are not symmetric upon $\theta \rightarrow \pi - \theta$ where θ denotes the angle of emission with respect to the axis of the electric field of the laser. This lack of symmetry is reminiscent of a corresponding violation of polar symmetry that has been predicted and observed under the condition that $\langle E(t)^3 \rangle_t \neq 0$, for two-color (2:1) multiphoton ionization of lowest order [24] or to arbitrary order [20,21]. The latter is a *quantum-mechanical* interference phenomenon, due to the fact that for a frequency ratio of 2:1 ionization populates even-parity as well as odd-parity states in the continuum that are degenerate in energy, and these states interfere as a function of their relative phase. We here consider the *classical* angular distributions generated by electrons that have been set free by ionization and later *rescatter* off their mother ions. The violations of polar symmetry in both cases are related insomuch as they both can be traced back to symmetries or lack thereof of the external laser field. For example, in both cases the violation of polar symmetry does not occur for a frequency ratio of 3:1 [or, more generally (2n+1):1]. In a realistic situation, both effects are present, in principle. However, the features we are interested in, the angular distributions of high-energy ATI which, classically, are exclusively due to backscattering should only be insignificantly affected by the aforementioned quantum interference effects. These might, in the classical picture that we consider, just introduce some angular bias in the initial velocity distribution (which we will put equal to zero). This will not have much of an effect particularly on the high-energy ATI peaks.

The paper is organized as follows. In the next section, we discuss the classical kinematics of rescattering electrons and draw the comparison to high-harmonic generation and two-step models where the electron leaves the field region without revisiting the ionic core. We confront the multiphoton regime at comparatively low intensities and the tunneling regime at high intensities. We relate certain symmetry properties of the laser field regarding the relative phase between the fundamental and the second harmonic to properties of the ATI spectrum. The third section displays numerical results for the distribution of the rescattered electrons with respect to energy and angle, both within the multiphoton and the tunneling regime. We also explain a graphical method that allows one to get a quick idea of what to expect, for arbitrary fields, and apply it to fields with frequency ratios of 3:1 and 3:2. In the last section, finally, we formulate our conclusions.

II. KINEMATICS OF RESCATTERING

We will consider a general linearly polarized field in the dipole approximation with vector potential $\mathbf{A}(t)=A(t)\hat{\mathbf{x}}$. The velocity of a charged particle in the presence of this field is

$$m\mathbf{v}(t)=\mathbf{p}-e\mathbf{A}(t), \tag{1}$$

where the canonical momentum $\mathbf{p}$ is a conserved quantity. We will restrict ourselves to the case where $\mathbf{v}(t_0)=0$ (this will be justified below) and gauges such that $\langle A(t) \rangle_t = 0$ ($\langle\ \rangle_t$ indicates averaging over time). All of the ensuing motion then takes place in the direction of the field so that

$$mv(t) \equiv mv_x(t) = e[A(t_0)-A(t)] \tag{2}$$

and

$$x(t)=\frac{e}{m}(t-t_0)A(t_0)-\frac{e}{m}\int_{t_0}^{t} d\tau\, A(\tau). \tag{3}$$

Here we have assumed that at $t=t_0$ the particle starts at the origin (with velocity zero). Depending on the value of t_0 it may return there at some later time $t_1 \equiv t_1(t_0)$ to be determined from

$$x(t_1)=0. \tag{4}$$

When the particle reenters the range of the potential it will scatter by some angle which, in general, is a function of its impact parameter. In our simplified description where we replace the binding potential in effect by a zero-range interaction and the particle starts with zero velocity at the position of the former (viz. the origin) the value of the impact parameter is always zero. It is then consistent to assume that the particle upon its return to the origin at time t_1 scatters by an angle θ_0 with respect to the negative x axis, where θ_0 is a uniformly distributed random quantity. This is the classical description of the quantum-mechanical fact that the scattering amplitude of a zero-range potential does not depend on the scattering angle. For times $t \geq t_1$ we then have

$$mv_x(t) = e[A(t_1) - A(t)] - e\cos\theta_0 |A(t_0) - A(t_1)|, \quad (5)$$

$$mv_y(t) = e\sin\theta_0 |A(t_0) - A(t_1)|, \quad (6)$$

where $0 \leq \theta_0 \leq \pi$. If just before its return to the origin the particle moves in the positive (negative) x direction then backscattering corresponds to $\theta_0 = 0$ ($\theta_0 = \pi$). For short pulses, the canonical momentum is conserved when the particle leaves the pulse and a particle that was scattered by the angle θ_0 arrives at the detector at the angle θ given by

$$\frac{\langle v_x(t)\rangle_t}{\langle v_y(t)\rangle_t} = \cot\theta = \cot\theta_0 - \frac{A(t_1)}{\sin\theta_0 |A(t_0) - A(t_1)|}. \quad (7)$$

Again for short pulses, the kinetic energy at the detector (outside the pulse) is

$$E_{\text{kin}} = \frac{m}{2}\langle v_x(t)^2 + v_y(t)^2\rangle_t - U_p$$
$$= \frac{e^2}{2m}\{A(t_0)^2 + 2A(t_1)[A(t_1) - A(t_0)](1 \pm \cos\theta_0)\}, \quad (8)$$

where the upper (lower) sign holds for $A(t_0) > A(t_1)$ [$A(t_0) < A(t_1)$] and

$$U_p = \frac{e^2}{2m}\langle A(t)^2\rangle_t \quad (9)$$

is the ponderomotive potential of the entire field. It can be checked that in either case the largest kinetic energies occur for backscattering. They are

$$E_{\text{kin}} = \frac{e^2}{2m}[2A(t_1) - A(t_0)]^2 \quad (10)$$

and they are assumed for $\theta_0 = \pi$ if $A(t_1) > A(t_0)$ and for $\theta_0 = 0$ if $A(t_1) < A(t_0)$. Notice that $\theta_0 = 0$ ($\theta_0 = \pi$) implies $\theta = 0$ ($\theta = \pi$). On the other hand, the energy of the electron upon its return to the origin (just before the rescattering) is

$$E_{\text{kin,return}} = \frac{e^2}{2m}[A(t_1) - A(t_0)]^2. \quad (11)$$

It is the maximum of this energy that determines the cutoff of high-harmonic production [9,10]. Comparison of Eqs. (10) and (11) demonstrates the possibility of additional energy gain by rescattering.

We note in passing that without rescattering the electron leaves the pulse with the velocity

$$mv = m\langle v(t)\rangle_t = eA(t_0) \quad (12)$$

and

$$E_{\text{kin}} = \frac{e^2}{2m}A(t_0)^2. \quad (13)$$

Equations (12) and (13) along with a source distribution such as given in Eq. (19) below constitute the two-step ("simpleman") model [7,8]. They have been used by Schuhmacher and collaborators to model their two-color experiments [14].

Introducing the indefinite integral of the vector potential

$$F(t) = \int^t d\tau\, A(\tau), \quad (14)$$

we may rewrite Eq.(4) which determines the return time t_1 as

$$F(t_1) = F(t_0) + (t_1 - t_0)F'(t_0). \quad (15)$$

If we are interested in the maxima of the backscattering energy (10) then we get a second equation by taking the derivative of Eq. (10) with respect to t_0,

$$A(t_1) = A(t_0) - 2(t_1 - t_0)E(t_1). \quad (16)$$

For the one-color field $A(t) = -A\sin\omega t$, Eqs. (15) and (16) can be reduced to the single trigonometric equation

$$\left(\frac{1}{\tau} - \cot\tau\right)\left(\frac{1}{2\tau} - \cot\tau\right) = 1 \quad (17)$$

for $\tau = \frac{1}{2}\omega(t_1 - t_0)$. Given τ, the remaining variable $\sigma = \frac{1}{2}\omega(t_1 + t_0)$ is determined from $\cot\sigma = \cot\tau - 1/\tau$. The solution of Eq. (17) that corresponds to a maximal backscattering energy (10) is $\tau = 2.153$ which yields $\sigma = -0.728$ and

$$E_{\text{kin,max}} = 10.007U_p. \quad (18)$$

At the corresponding release time $\omega t_0 = \sigma - \tau$ the electric field is just 3.5% below its peak value. Consequently, in the one-color case this maximal backscattering energy is emitted even for very high intensities of the laser field. Below, we will exhibit results of a numerical solution of the one-dimensional Schrödinger equation which demonstrate that the classical cutoff energy (18) is well obeyed by the calculated high-energy ATI spectra.

It is interesting to compare the times t_0 that yield maximal backscattering energies to those that produce the highest kinetic energy for the returning electron, i.e., the highest frequencies in harmonic emission. These latter times are determined by two equations just like Eqs. (15) and (16) except that the factor of 2 in Eq. (16) is absent. The solutions are [25] $\tau = 2.043$ and $\sigma = \pi/4 = -0.785$ for which the electric field is 5% below its peak value. The close proximity of the times that are optimal for high-harmonic generation and

those that cause the highest backscattering energies will extend to the two-color field (20). However, the electric field will not always be near its peak for those times.

For a two-color field such as given in Eq. (20) below we will turn to numerical methods. We will proceed as follows. We sample a very large number of electron trajectories treating both the release time t_0 and the scattering angle θ_0 as random quantities with a uniform distribution. For each t_0, we solve Eq. (4) for t_1 and then calculate θ and $E_{\rm kin}$ from Eqs. (7) and (8). Depending on t_0, Eq. (4) has no, one, or any number of solutions corresponding to the number of returns of the free-electron trajectory to the origin. (To be precise, any *odd* number, unless we count the situation of the electron turning around at the very position of the origin as *one* return.) For the results presented in this paper, we only considered the *first* return, i.e., we chose the solution t_1 closest to t_0. The significance of the later returns is an interesting question which we will come back to below. We have used a uniform distribution of release times, since, of course, time proceeds uniformly. However, at some times more electrons may be released than at others. The rate of injection of electrons in the continuum is, in general, a function of the absolute value of the field at that time: $R(\mathrm{t}) \equiv \mathrm{R}(|E(t)|)$. The contributions from a given t_0 are assigned a weight proportional to this rate of injection. In this paper we will consider two limiting cases: (i) The rate of injection does not depend on the field; this corresponds to the comparatively-low-energy multiphoton regime. In this case, actually, the electron starts with a certain nonzero energy $N\hbar\omega - I_p$ where I_p is the field-free ionization potential. This energy is very small compared to the energies after rescattering and we have ignored it, assuming that the initial velocity is zero. (ii) In the tunneling regime, the rate of injection is a strongly peaked function of $|E(t)|$, for example [26],

$$R(t) \sim |E(t)|^{-1} \exp\left(-\frac{2}{3|E(t)|}\right) \tag{19}$$

in atomic units. In this case, it appears natural to assume that the electron starts with a velocity of zero; see, however, Ref. [11].

In this paper we will mostly consider the electric field

$$E(t) = \omega A[\cos\omega t + \cos(2\omega t + \phi)] \tag{20}$$

corresponding to the vector potential

$$A(t) = -A[\sin\omega t + \tfrac{1}{2}\sin(2\omega t + \phi)]. \tag{21}$$

This field has the following symmetries:

$$\text{(I)}\quad \phi \to \phi + \pi,\ t \to t + \frac{\pi}{\omega} \Rightarrow E(t) \to -E(t),\ A(t) \to -A(t), \tag{22}$$

$$\text{(II)}\quad \phi \to -\phi,\ t \to -t \Rightarrow E(t) \to E(t),\ A(t) \to -A(t). \tag{23}$$

The symmetry (I) implies that when the phase ϕ is changed by 180° and, at the same time, the origin of time is shifted by the specified amount (a procedure which has no physical significance) this corresponds to reversing the x direction. That is, two fields (20) whose phases ϕ differ by 180° yield the same ATI spectra except that the backward and the forward directions are interchanged. The consequences of symmetry (II) are somewhat more subtle, as we will now explain. The reason is that time reversal is included. In order to obtain the observed spectra we have to sum over all possible initial times t_0 as discussed above. Since we sample the release times randomly, time reversal does not seem to make any difference as long as the rate of injection $R(t)$ is a function of just the field. However, a moment of further thought makes clear that time reversal interchanges the temporal order of the release time t_0 and the return time t_1, but, of course, the first has to precede the second. Hence, the consequences of the symmetry (II) are different for electrons that are or that are not rescattered. For those that are not, two fields that differ by the sign of the phase ϕ yield ATI spectra with the forward and backward direction interchanged since $A(t_0) \to -A(t_0)$ in Eq.(12). For the spectra of the rescattered electrons, however, there is no relationship when the sign of the phase ϕ is reversed. Notice that for the more general field $E(t) = E_1\cos(n_1\omega t + \phi_1) + E_2\cos(n_2\omega t + \phi_2)$ the relevant phase which controls the effects under discussion is $n_1\phi_2 - n_2\phi_1$ in place of ϕ.

These considerations carry over to a quantum description. KFR theories [19] or two-step models [5] produce spectra obeying the $\phi \to -\phi$, $\hat{\mathbf{x}} \to -\hat{\mathbf{x}}$ symmetry since they do not account for rescattering. Three-step models, on the other hand, do not since they do. As a consequence, the total ionization rates for individual ATI peaks which sum over all directions are invariant upon $\phi \to -\phi$ insomuch as rescattering is ignored, but not in general. This holds both in a classical and in a quantum-mechanical description.

III. RESULTS AND DISCUSSION

Figure 1 shows density plots of the number $n(E_{\rm kin}, \theta)$ of rescattered electrons in the multiphoton (left-hand half) and in the tunneling regime (right-hand half). In the multiphoton case, injection occurs uniformly in time; in the tunneling case, we used the injection rate (19) with the electric field (20) and $E_0 = \omega A = 0.015$ a.u. This is a field of comparatively low intensity, but yields for demonstrational purposes a rate of injection that is very strongly peaked at the maxima of the electric field. For the multiphoton case, the intensity is completely incorporated just by scaling $E_{\rm kin}$ with respect to U_p. Results are given for several phases between 0 and π. These can be used to generate plots for phases outside this interval with the help of the symmetry (22). It must be kept in mind that the figures only refer to the *rescattered* electrons. In order to obtain the total observable distributions the contributions from those electrons that do not rescatter must be added. Equation (13) shows, however, that classically their energies cannot exceed $2U_p$. Hence, most of Fig. 1 remains unaffected. A most conspicuous feature of these density plots consists of the potentially very large energies of the backscattered electrons. Around $\phi = \pi/2$ they come close to $21U_p$, to be compared to the maximum of $10.007U_p$ [Eq. (18)] in the one-color case. For this phase the vector potential, not the electric field, attains its maximal value at appropriate times. The bell-shaped boundaries in Fig. 1 reflect the factor of $1 \pm \cos\theta_0$ in Eq. (8). They are, however, distorted as

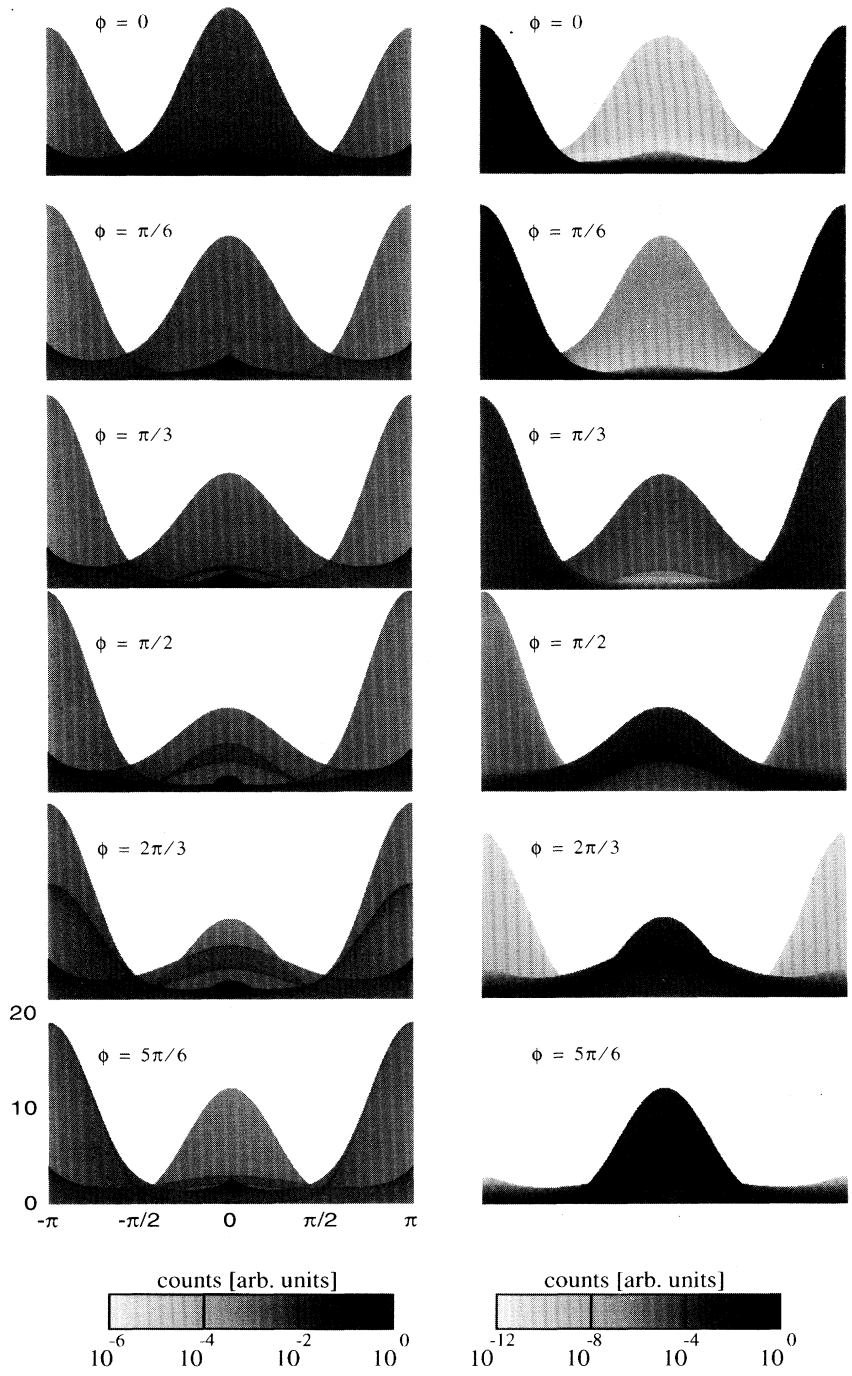

FIG. 1. Density plot of the number $N(E_{\text{kin}},\theta)$ of backscattered electrons emitted with kinetic energy E_{kin} at an angle θ with respect to the negative x axis. The angle θ is plotted along the horizontal axis from $-180°$ to $180°$. (Allowing for negative angles was just a test of the numerical accuracy; the plots ought to be completely symmetric with respect to $0°$.) The kinetic energy is plotted along the vertical axis from 0 to $21U_p$. The plots are for phases from $\phi=0$ to $\phi=150°$ in steps of $30°$. Left-hand half: the field intensity corresponds to the multiphoton regime, so that the rate of electron injection is uniform. Right-hand half: the field intensity corresponds to the tunneling regime, so that electrons are preferentially injected at the peaks of the electric field. Notice how the general shape of the density plots is identical in both regimes while the intensity corresponding to the respective number of electrons is different owing to the field dependence of the rate of injection in the right-hand half. The gray scale which specifies the electron numbers covers 6 orders of magnitude in the left-hand half of the figure and 12 orders in the right-hand half. In each case, the gray-scale calibration is given at the bottom of the figure.

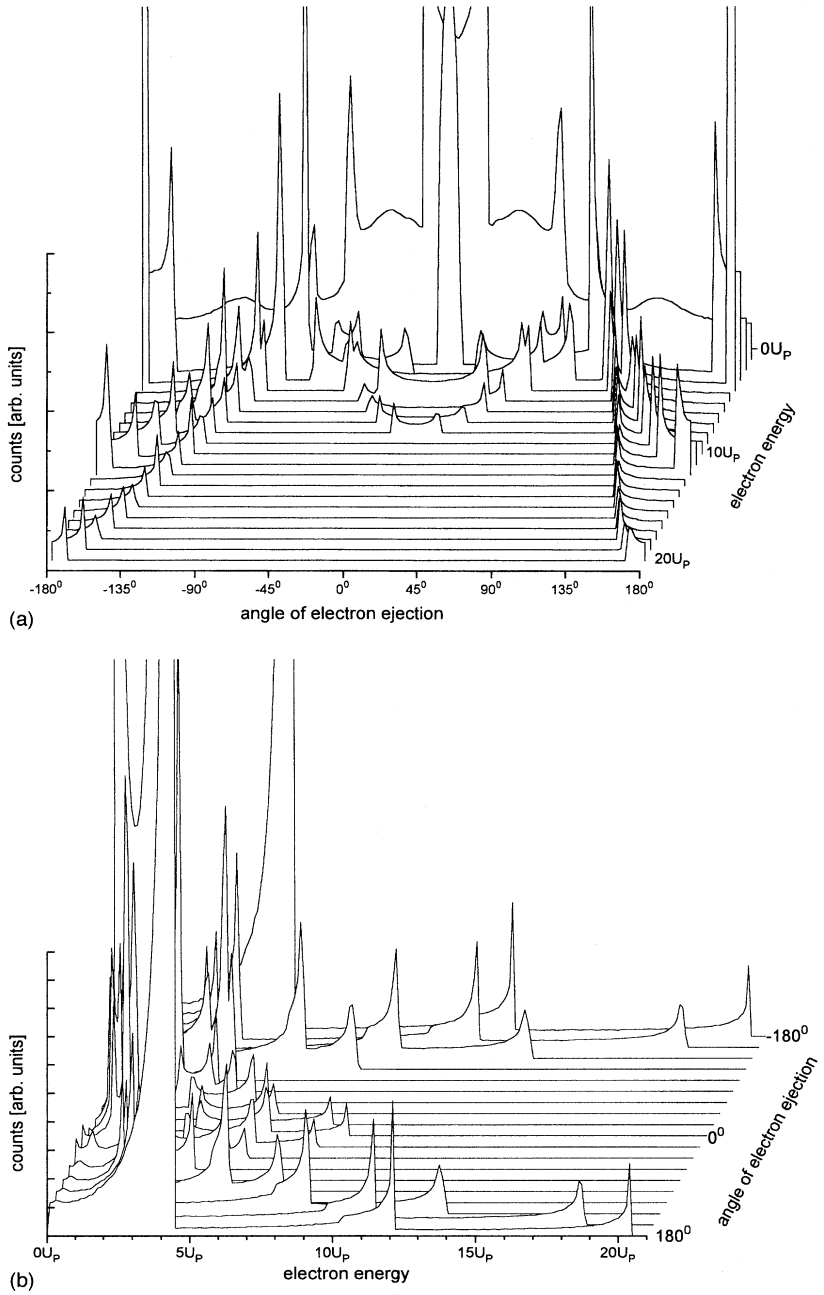

FIG. 2. Angular distributions for fixed energy (a) and energy distributions for fixed scattering angle (b) for the multiphoton regime (left-hand half of Fig. 1) for $\phi = 2\pi/3$. The distributions ought to be symmetric about an angle of electron ejection of 0°. Deviations from this symmetry are due to the finite sampling size.

a consequence of Eq. (7) as they are plotted versus the observed angle θ rather than the scattering angle θ_0 at the origin. Even though θ_0 is uniformly distributed, owing to the subsequent acceleration by the laser electric field the observed distributions are concentrated around this direction, that is, $\theta = 0$ and $\theta = \pi$. Since there is no acceleration at right angles to it, the maximal energy at $\theta = \pi/2$ approximately gives the maximal energy $(e^2/2m)A(t_1)^2$ of the returning electron which is related to the cutoff of high-harmonic emission. This energy does depend on ϕ, though not very dramatically, and is much smaller than the maximal rescattering energies. Horizontal cuts through the density plots, at $E_{\text{kin}} =$ const, produce the angular distributions at constant energy. An example is given in Fig. 2(a). They display sharp cutoffs at certain angles $\theta_{\min}(E_{\text{kin}})$ and $\theta_{\max}(E_{\text{kin}})$ for which the distribution drops to zero after a pronounced spike. These features are familiar from the one-color case [12]. Experimentally, they have been observed as the sidelobes or rings that make up the so-called anomalous angular distributions [2,3]. The present two-color case adds several new features. As discussed already, the forward-backward symmetry of the angular distributions is lost. For some phases ϕ, there are several of these cutoffs at different angles. This means that several sidelobes should appear in the angular distributions at different angles. A nice example occurs for $\phi = 2\pi/3$, the value picked for Fig. 2. The graphical discussion to be explained below will trace these cutoffs to different emission times t_0. A vertical cut, at $\theta =$ const, yields the energy dis-

tributions at constant angle, cf. Fig. 2(b). Again there are sharp cutoffs corresponding to maximal energies that can be emitted in a given direction, and again, for appropriate phases, there are several such cutoffs for a given angle.

Interestingly, the one-color experiments, see Ref. [2] and in particular Ref. [3], have displayed very well defined angular cutoffs, in good quantitative agreement with the predictions of the classical calculation of Ref. [12]. On the other hand, the energy cutoffs that result from classical kinematics ($2U_p$ for the direct electrons and $10U_p$ for the backscattered electrons in the one-color case) are visible in experiments, too, as well as in numerical simulations, but appear to be greatly smoothed by quantum mechanics.

There are, again in the one-color case, two major areas where the classical model [12] disagrees with the data [2,3]. First, the classical model underestimates rescattering in the field direction. Second, it yields angular cutoffs leading to rings in the angular distributions for *all* rescattering energies, unlike the experiments which show them only in a rather small window around an energy of about $8U_p$. The question is whether these discrepancies point to the presence of some genuinely quantum-mechanical mechanism in the data which is completely unaccounted for by the classical model or, alternatively, whether they can just be attributed to the general observation that quantum mechanics tends to "smooth" the classical results. While we do not attempt to resolve this question we will present some arguments in favor of the latter possibility. The experimental fact that the rings are not visible for energies much below $8U_p$ may be traceable to a dominance of the direct electrons in this energy region. Recall that the classical cutoff of $2U_p$ for the direct electrons is not at all well respected by quantum mechanics. Hence, direct electrons may drown the contributions from the rescattered electrons including the rings for energies much higher than $2U_p$ and, possibly, up to close to $8U_p$. On the other hand, for energies much in excess of $8U_p$, the classical angular cutoffs move closer and closer to the field direction. As a consequence, due to quantum-mechanical smoothing they may no longer remain recognizable as separate rings. Analogous discrepancies can be expected between the results of the classical two-color model of this paper and future experiments.

The right-hand half of Fig. 1 shows what happens when the intensity is raised into the tunneling regime. In this realm electrons are preferentially emitted near those times t_0 where the electric field is at its maximum as opposed to the lower intensities where the emission is uniform in time. For example, for phases $\phi=30°$, 60°, and 90°, there are two peaks of the electric field of nearly equal height within one periodicity interval. Hence, even in the tunneling regime there is emission in both the positive and the negative direction and not much happens when the intensity increases from one regime to the other. On the other hand, for phases $\phi=0°$, 120°, and 150°, there is just one dominant peak and essentially only emission in one direction survives in the tunneling regime. For an illustration of the respective fields in these two cases, compare Fig. 3 for $\phi=0$ and $\phi=\pi/2$. For the same reason, the multiple spikes or cutoffs in the energy or angular distributions mentioned above disappear in the tunneling regime. The energy distributions of the high-energy two-color ATI peaks for appropriate phases provide a striking signature of ionization occurring through tunneling as opposed to the multiphoton mechanism.

It is instructive to gain some physical understanding of the kinematics of Figs. 1 and 2 by a simple graphical method. Looking back at Eq. (15) we realize that it is amenable to a simple graphical solution. For given t_0, we can determine t_1 by intersecting $F(t)$ with its tangent at t_0. In Fig. 3 we plot, for the field (20), the quantity $\omega F(t)/A$ along with the scaled field $E(t)/\omega\, A$ and the scaled vector potential $A(t)/A$ for $\phi=0$ and $\phi=90°$. From Eqs. (9) and (10) the kinetic energy for the case of backscattering is, for the field (20),

$$\frac{E_{\rm kin}}{U_p}=\frac{8}{5A^2}[2A(t_1)-A(t_0)]^2, \tag{24}$$

where t_1 has been determined graphically as described above and $A(t_0)$ and $A(t_1)$ can be read off from the graph. This energy becomes maximal approximately for times t_1 such that $|A(t_1)|$ is maximal. The graphical procedure is illustrated in Fig. 3(a) for the case $\phi=0$. The figure shows that there are two small regions of the release time, around t_0 and $\tilde{t}_0$, which will give rise to maximal backscattering energies. We infer from the figure that $A(t_1)<A(t_0)$ so that backscattering in this case corresponds to $\theta_0=0$, while $A(\tilde{t}_1)>A(\tilde{t}_0)$ so that backscattering means $\theta_0=\pi$ in this latter case. (Only t_0 and t_1 are explicitly drawn in the figure in order not to overburden it.) From the values of $A(t_0)$ etc. we can estimate with the help of Eq. (10) that $E_{\rm kin}(t_0)\sim 15U_p$ (for $\theta_0=0$), slightly larger than $E_{\rm kin}(\tilde{t}_0)\sim 13U_p$ (for $\theta_0=\pi$). All of these features can be seen in Fig. 1 which displays the results of the exact numerical calculation. If the release times are uniformly distributed then the contributions coming from release at t_0 and $\tilde{t}_0$ have about the same weight, and we expect them to have about the same impact on the spectrum. This can be seen in the left-hand half of Fig. 1. If, however, the electron enters the continuum via tunneling then the contribution from the release time $\tilde{t}_0$ where the electric field is near its maximum is by far dominant. Indeed, the right-hand half of Fig. 1 which is based on weighing the release time according to Eq. (19) exhibits the contribution from $\tilde{t}_0$ to be completely dominant with just a trace left from emission at time t_0. For $\phi=\pi/2$, on the other hand, the magnitudes of the peak values of the electric field are identical, and, consequently, there is little change in the electron spectrum when the increasing field intensity takes one from the multiphoton into the tunneling regime (insomuch as one is only interested in high-energy backscattering; the spectrum at lower energies does change.)

Field configurations with frequency ratios other than 2:1 provide variations of the same theme. For example, for the field

$$E(t)=E_1\cos\omega t+E_3\cos(3\omega t+\phi), \tag{25}$$

for arbitrary amplitudes E_1 and E_3 the angular distributions including rescattering are symmetric upon $\theta\rightarrow\pi-\theta$. The reason is that under $\omega t\rightarrow\omega t+\pi$ the field as well as the vector potential change sign. Hence the forward and backward directions are equivalent. The polar asymmetry due to quantum interference [20,24] vanishes in this case, too. The

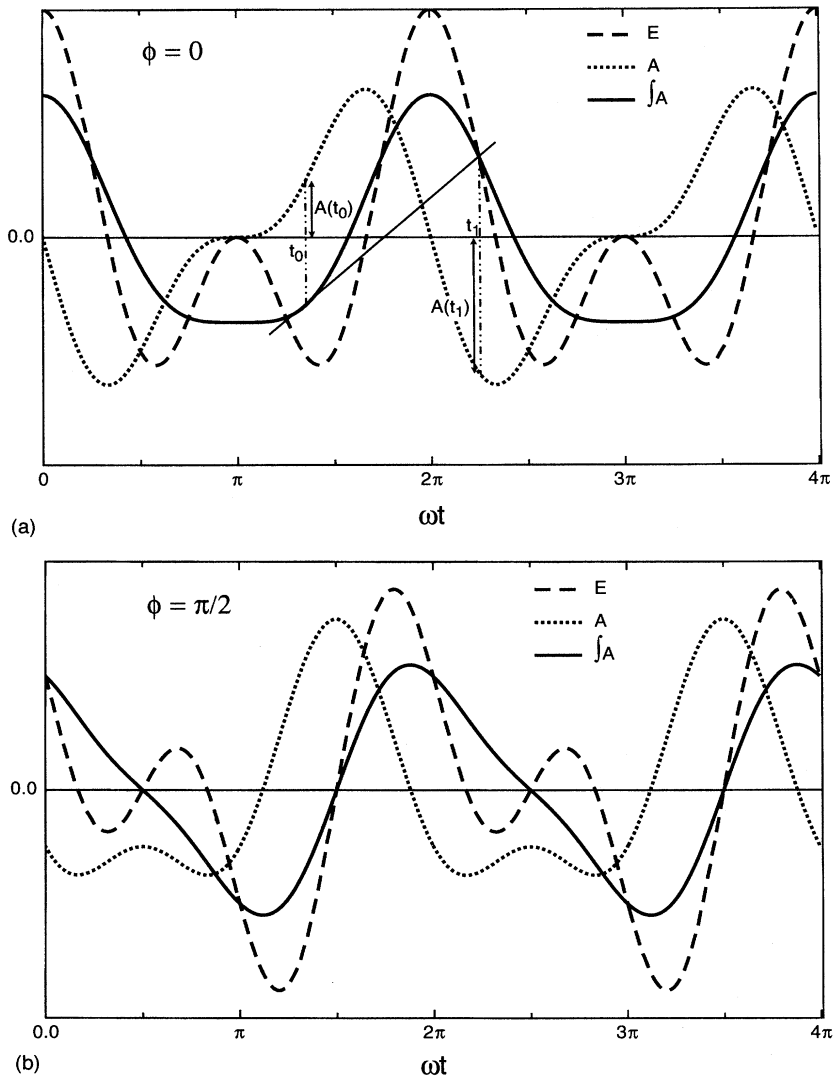

FIG. 3. Illustration of the graphical method explained in the text to explore the kinematics. Plotted are the vector potential $A(t)/A$ (solid line), the electric field $E(t)/\omega A$ (dashed line), and the integral of the vector potential $\omega F(t)/A$ (dotted line) for the field (20) with $\phi=0$ (a) and $\phi=\pi/2$ (b). For $\phi=0$ (a), the vector potential is symmetric with respect to the horizontal axis (up to a shift) while the electric field is not. Extremal backscattering energies occur for electron emission near $\omega t_0\approx 4.2$ and $\omega\tilde{t}_0\approx 6.4$, and are of comparable magnitude. Since the electric field at $\tilde{t}_0$ is much stronger than at t_0, in the tunneling regime emission at $\tilde{t}_0$ is dominant over emission at t_0. (Only the release time t_0 and the graphical construction leading to the return time t_1 are explicitly shown; the reader is invited to draw the remaining lines if desired.) For $\phi=\pi/2$ (b), the shape of the field is symmetric, but the vector potential is not. Extremal backscattering energies occur for emission near times $\omega t_0=3.6$ and 3.8, as well as near $\omega t=6.1$. (These times are not displayed in the figure.) The former two yield return times t_1 where the vector potential reaches its two negative extrema and backscattering in the direction of $\theta=0$. Emission at $\omega t_0\approx 6.1$ leads to by far the largest backscattering energy in the direction of $\theta=\pi$. The electric field is comparable at all these times, so there is little change in going from the multiphoton to the tunneling regime. Compare with Fig. 1.

same holds true for any odd integer frequency ratio. Other frequency ratios lead to more involved phenomena. In Fig. 4 we plot the analog of Fig. 3 for the field

$$E(t)=2\omega A(\cos 2\omega t+\cos(3\omega t+\phi)) \tag{26}$$

for $\phi=0$. A Floquet calculation for this field has been carried out in Ref. [27]. In general, this field is invariant under $\omega t\rightarrow\omega t+\pi$ and $\phi\rightarrow\phi+\pi$. Hence, the ATI spectra of two fields whose relative phases differ by π are identical. Upon $\omega t\rightarrow\omega t+\pi/2$ and $\phi\rightarrow\phi-\pi/2$ both the field (26) and its vector potential change sign. Consequently, the respective ATI spectra are the same if forward and backward directions are interchanged. In particular, for $\phi=0$, Fig. 4 shows, along the lines of a graphical discussion as exemplified above, that the four highest maxima of $|A(t)|$ within one periodicity interval of 2π will each give rise to one particular maximal rescattering energy, two for $\theta_0=\pi$, and two more for $\theta_0=0$. The electric field has its most pronounced maximum at $t=0$, the other ones being substantially smaller. This im-

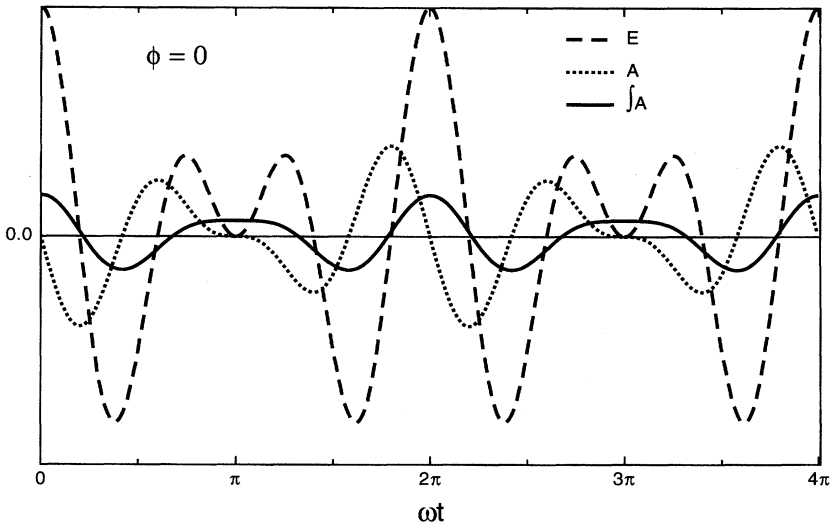

FIG. 4. Same as Fig. 3, but for the 2:3 field (26) with $\phi=0$. See the discussion in the text.

plies that out of the four just mentioned maximal backscattering energies in the tunneling limit the one which is generated by an electron set free at about this time $[t_0 \approx 0 \pmod{2\pi}]$ will be strongly dominant. This maximum occurs for $\theta_0=\pi$, and its energy is comparatively low. It is interesting to notice that the function $F(t)$ [cf. Eq. (14)] has an extended flat section for about $2.6 \leq \omega t_0 \leq 3.4 \pmod{2\pi}$. This means that all of the electrons set free within this range will return close to the time $\omega t_1 \approx 5.8$. This leads to a fairly narrow range of backscattering energies which will dominate the spectrum in the multiphoton regime. Since, however, the electric field is rather small within this range of initial times the contribution of these electrons will become less and less important when the field intensity approaches the tunneling regime.

The graphical discussion makes it very clear that the electron may return to the core more than once, in fact, any number of times depending on its time of release. In a completely classical scenario, upon its return it will invariably rescatter, so that unless it scatters exactly in the forward or backward direction it will never return again. Hence, we have disregarded these higher return times. However, quantum mechanically, this appears to be different. In analytic expressions related to high-harmonic generation [25] and ATI rescattering [22] these higher return times can be identified very clearly and equally clearly have some effect on the results. Whether or not they lead to identifiable qualitative experimental signatures is an interesting open question; for a discussion in the one-color case, see Ref. [12].

For two-color high-energy ATI there are neither real nor numerical experiments that could serve as a testing ground for these classical features. However, Fig. 5 shows the results of a numerical solution of the one-dimensional Schrödinger equation in the presence of a one-color field for a range of intensities. The method of solution has been described earlier [4]. In each case, we can see that the classical cutoff for backscattering of approximately $10U_p$ [cf. Eq. (18)] is very well respected, particularly so for the higher intensities corresponding to higher electron energies. For the highest intensity, the classical cutoff of "ordinary" ATI at $2U_p$ [cf. Eq. (13) which yields a maximum of $2U_p$ for a one-color field] is very noticeable as well.

The graphical method employed above could also be used for a discussion of the cutoff energy of two-color high-

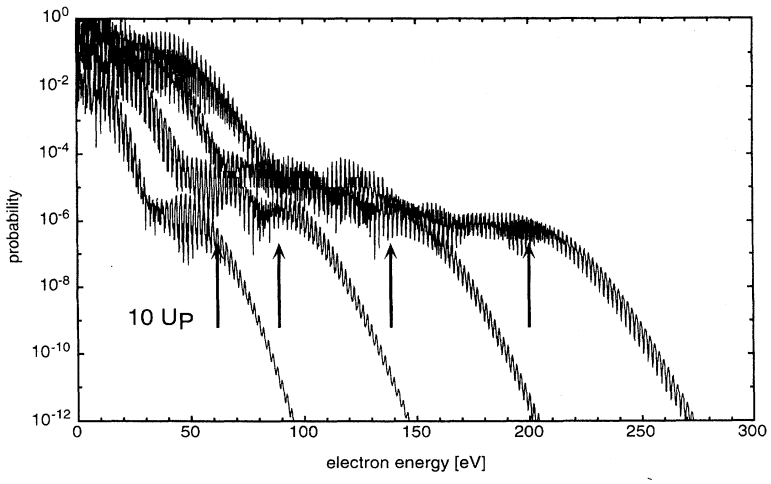

FIG. 5. ATI spectra calculated for the one-dimensional model potential $V(x) = -(1+x^2)^{1/2}$ for several ponderomotive potentials between 6 and 20 eV. The maximal classical backscattering energy is marked by an arrow in each case.

harmonic generation by parallel linearly polarized fields [28]. It makes it very clear why in this case there is no simple cutoff law of the form $E_{\max}=I_p+\alpha U_p$ with α some (phase-dependent) constant or a similar expression with a linear dependence on the ponderomotive energies of the two fields separately. For given t_0, we can again determine the return time t_1 and then estimate t_0 such as to obtain a maximal return energy. However, several local maxima corresponding to different release times t_0 will exist and when going from the multiphoton to the tunneling regime they will become weighted with the rate of injection (19). Hence, while the *positions* of the various maxima remain proportional to the ponderomotive potential their *quantitative significance* may become a highly nonlinear function of the electric field. This makes it impossible to write down a simple cutoff formula that covers the entire range of intensities.

IV. CONCLUSIONS

We have investigated classical rescattering effects of ionized electrons returning to the core for the case of a superposition of a linearly polarized monochromatic field and its second harmonic, with a well-defined relative phase. A crucial point is the fact that the ionization rate depends predominantly on the electric field while the distribution of the electron energies in the continuum is determined by the vector potential. For a sinusoidal one-color field, the relation between electric field and vector potential is rigid and leaves no room for tampering. For a two-color field, it depends on the relative phase and can thereby be manipulated allowing for far-reaching control of the electron spectrum. This provides an interesting example of what is called coherent control in photochemistry [29]. The features that are due to this additional freedom include the following: The energies of the rescattered electrons can be much higher than in the one-color case, up to $21U_p$ as compared to just $10U_p$ in the one-color case. This is due to the possibility of more efficient acceleration for a suitably tailored field. Since the forward-backward symmetry of the vector potential is lost, so is the corresponding symmetry of the electron spectrum. As the shape of the field as a function of time is more complicated there are possible relations between the release time t_0 and the return time t_1 that give rise to more structure in the electron spectrum such as additional side lobes or rings in the angular distributions. When the phase between the two components of the entire field changes sign, for electrons that leave the field region without rescattering this is equivalent to the backward-forward interchange. For electrons that do rescatter, there is no such relationship. Hence, the invariance of the total emission rate with respect to $\phi\rightarrow-\phi$ or the lack thereof provides a good test for the significance of rescattering [14]. The spectrum of the rescattered electrons is, for appropriate phases, very sensitively dependent of the ionization mechanism. Whole sequences of electron energies disappear from the spectrum when the tunneling limit is approached, viz. those where the electric field at the time of emission is low. This is a very qualitative effect that would give a clear indication of how ionization occurs.

To what extent the results of this entirely classical model can be expected to hold in a quantum-mechanical world remains to some extent open. In the one-color case, we have observed good agreement with the experimental data in some features along with discrepancies in others [12]. In any event, the classical model investigated in this paper gives some hints as to what can be expected. A two-color environment will provide a much more stringent test of the relevance of these classical semi-free-electron models to multiphoton phenomena than a monochromatic field can yield. In particular, this will apply for field geometries that are no longer one dimensional. This aspect has not been touched upon in this paper.

ACKNOWLEDGMENTS

We enjoyed beneficial discussions with M. Kleber, P. Lambropoulos, A. Lohr, and W. Nicklich. W. B. appreciates the hospitality of the theory division of the Physics Department of the Technical University of Munich. W. B. also acknowledges partial support by the Sonderforschungsbereich SFB 338 of the Deutsche Forschungsgemeinschaft.

[1] P. Agostini, F. Fabre, G. Mainfray, G. Petite, and N. K. Rahman, Phys. Rev. Lett. **42**, 1127 (1979); for a recent review, see H. G. Muller, P. Agostini, and G. Petite, in *Atoms in Intense Fields*, edited by M. Gavrila (Academic, Boston, 1992), p. 1.

[2] B. Yang, K. J. Schafer, B. Walker, K. C. Kulander, P. Agostini, and L. F. DiMauro, Phys. Rev. Lett. **71**, 3770 (1993).

[3] G. G. Paulus, W. Nicklich, and H. Walther, Europhys. Lett. **27**, 267 (1994).

[4] G. G. Paulus, W. Nicklich, Huale Xu, P. Lambropoulos, and H. Walther, Phys. Rev. Lett. **72**, 2851 (1994).

[5] W. Becker, R. R. Schlicher, and M. O. Scully, J. Phys. B **19**, L785 (1986).

[6] H. G. Muller, Comments At. Mol. Phys. **24**, 355 (1990).

[7] H. B. van Linden van den Heuvell and H. G. Muller, in *Multiphoton Processes*, edited by S. J. Smith and P. L. Knight, Studies in Modern Optics No. 8 (Cambridge University Press, Cambridge, 1988), p. 25.

[8] P. B. Corkum, N. H. Burnett, and F. Brunel, in *Atoms in Intense Fields*, edited by M. Gavrila (Academic, Boston, 1992), p. 109.

[9] K. C. Kulander, K. J. Schafer, and J. L. Krause, in *Super-Intense Laser-Atom Physics*, Vol. 316 of *NATO Advanced Study Institute: Series B: Physics,* edited by B. Piraux, A. L'Huillier, and K. Rzążewski (Plenum, New York, 1993), p. 95.

[10] P. B. Corkum, Phys. Rev. Lett. **71**, 1994 (1993).

[11] W. Becker, A. Lohr, and M. Kleber, Quantum Semiclass. Opt. **7**, 423 (1995).

[12] G. G. Paulus, W. Becker, W. Nicklich, and H. Walther, J. Phys. B **27**, L703 (1994).

[13] P. A. Golovinskiy, Laser Physics **3**, 280 (1993).

[14] D. W. Schuhmacher, F. Weihe, H. G. Muller, and P. H. Bucksbaum, Phys. Rev. Lett. **73**, 1344 (1994).

[15] H. G. Muller, P. H. Bucksbaum, D. W. Schuhmacher, and A. Zavriyew, J. Phys. B **23**, 2761 (1990).

[16] A. Szöke, K. C. Kulander, and J. N. Bardsley, J. Phys. B **24**, 3165 (1991).
[17] K. J. Schafer and K. C. Kulander, Phys. Rev. **45**, 8026 (1992).
[18] R. M. Potvliege and P. H. G. Smith, J. Phys. B **25**, 2501 (1992).
[19] L. V. Keldysh, Zh. Éksp. Teor. Fiz. **47**, 1945 (1964) [Sov. Phys. JETP **20**, 1307]; F. H. M. Faisal, J. Phys. B **6**, L89 (1973); H. R. Reiss, Phys. Rev. A **22**, 1786 (1980).
[20] N. B. Baranova, B. Ya. Zeldovich, A. N. Chudinov, and A. A. Shul'ginov, Zh. Éksp. Teor. Fiz. **98**, 1857 (1990) [Sov. Phys. JETP **71**, 1043 (1990)]; N. B. Baranova, H. R. Reiss, and B. Ya. Zeldovich, Phys. Rev. A **48**, 1497 (1993).
[21] V. A. Padzersky and V. A. Yurovsky, Phys. Rev. A **51**, 632 (1995).
[22] W. Becker, A. Lohr, and M. Kleber, J. Phys. B **27**, L325 (1994); **28**, 1931 (1995).
[23] M. Lewenstein, K. C. Kulander, K. J. Schafer, and P. H. Bucksbaum, Phys. Rev. A **51**, 1495 (1995).
[24] D. Z. Anderson, N. B. Baranova, K. Green, and B. Ya. Zel'dovich, Zh. Éksp. Teor. Fiz. **102**, 397 (1992) [Sov. Phys. JETP **75**, 210 (1992)].
[25] W. Becker, S. Long, and J. K. McIver, Phys. Rev. A **50**, 1540 (1994).
[26] L. D. Landau and E. M. Lifshitz, *Quantum Mechanics* (Pergamon, London, 1978).
[27] R. M. Potvliege and P. H. G. Smith, Phys. Rev. A **49**, 3110 (1994).
[28] H. Eichmann, A. Egbert, S. Nolte, C. Momma, B. Wellegehausen, W. Becker, S. Long, and J. K. McIver, Phys. Rev. A **51**, R3414 (1995).
[29] M. Shapiro, J. W. Hepburn, and B. Brumer, Chem. Phys. Lett. **149**, 451 (1988); S. M. Park, Sh.-P. Lu, and R. J. Gordon, J. Chem. Phys. **94**, 8622 (1991); C. Chen and D. S. Elliot, Phys. Rev. Lett. **65**, 1737 (1990).

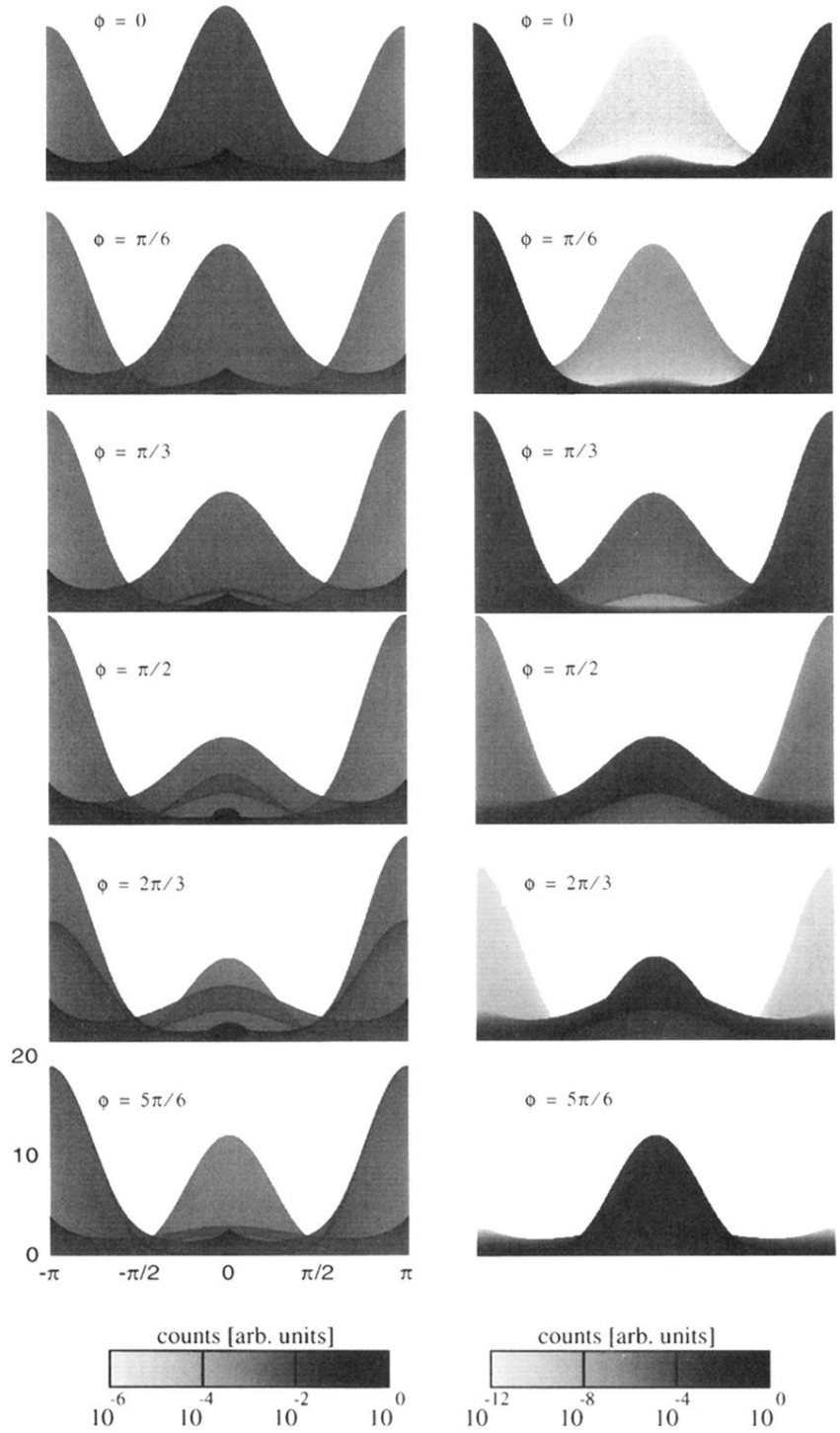

FIG. 1. Density plot of the number $N(E_{\text{kin}}, \theta)$ of backscattered electrons emitted with kinetic energy E_{kin} at an angle θ with respect to the negative x axis. The angle θ is plotted along the horizontal axis from $-180°$ to $180°$. (Allowing for negative angles was just a test of the numerical accuracy; the plots ought to be completely symmetric with respect to $0°$.) The kinetic energy is plotted along the vertical axis from 0 to $21U_p$. The plots are for phases from $\phi = 0$ to $\phi = 150°$ in steps of $30°$. Left-hand half: the field intensity corresponds to the multiphoton regime, so that the rate of electron injection is uniform. Right-hand half: the field intensity corresponds to the tunneling regime, so that electrons are preferentially injected at the peaks of the electric field. Notice how the general shape of the density plots is identical in both regimes while the intensity corresponding to the respective number of electrons is different owing to the field dependence of the rate of injection in the right-hand half. The gray scale which specifies the electron numbers covers 6 orders of magnitude in the left-hand half of the figure and 12 orders in the right-hand half. In each case, the gray-scale calibration is given at the bottom of the figure.